第 28 卷第 12 期 无 机 化 学 学 报 Vol.28 No.12
2012 年 12 月 CHINESE JOURNAL OF INORGANIC CHEMISTRY 2573-2580

锰源对燃烧法制备 5V 级正极材料 $LiNi_{0.5}Mn_{1.5}O_4$ 的影响

聂 翔[1] 郭孝东*,[1] 钟本和[1] 刘 恒[2] 方为茂[1]
([1]四川大学化学工程学院,成都 610065)
([2]四川大学材料科学与工程学院,成都 610065)

摘要: 以硝酸锰和醋酸锰,采用蔗糖燃烧法制备锂离子电池正极材料 $LiNi_{0.5}Mn_{1.5}O_4$ 通过 XRD、SEM、粒径分布测试、循环伏安、恒流充放电测试以及交流阻抗等方法,研究了醋酸锰和硝酸锰对产物的结构、形貌、粒径及电化学性能的影响。XRD 测试结果表明样品的结构都为立方尖晶石型,属于 *Fd*3*m* 空间群。不同的锰源对材料的粒径及粒径分布有很大的影响。以醋酸锰为原料制得的材料的粒径较小并且分布更均匀,有利于锂离子的脱出和嵌入从而提高电化学性能。以醋酸锰为锰源制得的 $LiNi_{0.5}Mn_{1.5}O_4$ 在 3.6~5.2 V 的充放电电压范围内的电化学性能更好,1C(1C=140.0 mA·g^{-1})倍率的首次放电容量为 144.5 mAh·g^{-1},循环 100 周后容量保持率为 96%,在 3C,5C,10C 以及 20C 的放电容量分别为 136.3,132.0,124.7 以及 96.6 mAh·g^{-1}。

关键词: 高电压正极材料; 蔗糖燃烧法; $LiNi_{0.5}Mn_{1.5}O_4$; 锰源
中图分类号: O646.21; TM912.9 **文献标识码**: A **文章编号**: 1001-4861(2012)12-2573-08

Effect of Mn Source on 5 V $LiNi_{0.5}Mn_{1.5}O_4$ Positive Electrode Materials Prepared by Combustion Method

NIE Xiang[1] GUO Xiao-Dong*,[1] ZHONG Ben-He[1] LIU Heng[2] FANG Wei-Mao[1]
([1]*College of Chemical Engineering, Sichuan University, Chengdu* 610065, *China*)
([2]*College of Materials Science and Engineering, Sichuan University, Chengdu* 610065, *China*)

Abstract: Sub-micrometric $LiNi_{0.5}Mn_{1.5}O_4$ cathode materials were prepared by sucrose combustion method with two different Mn sources. The effect of manganese acetate and manganese nitrate on the crystal structure, morphology, particle size and electrical performance of the prepared samples was evaluated by X-ray diffraction (XRD), scanning electron microscopy (SEM), particle size analysis, cyclic voltammetry (CV), galvanostatic charge-discharge test and electrochemical impedance spectroscopy (EIS). XRD analysis shows that the structure of both samples is a typical cubic spinel with *Fd*3*m* space group. The particle size and the distribution of the $LiNi_{0.5}Mn_{1.5}O_4$ powder are strongly influenced by Mn source. The materials prepared by manganese acetate have smaller particle size and narrower particle size distribution, which can facilitate Li ions extraction and insertion. Furthermore, the sample $LiNi_{0.5}Mn_{1.5}O_4$ prepared by manganese acetate has better electrochemical performances. An initial specific capacity of 144.5 mAh·g^{-1} at 1C in the voltage range of 3.6~5.2 V, 96% of the initial capacity after 100 cycles is maintained, and capacities of 136.3, 132.0, 124.7 and 96.6 mAh·g^{-1} are achieved at the rate of 3C, 5C, 10C and 20C, respectively.

Key words: high voltage cathode materials; sucrose combustion method; $LiNi_{0.5}Mn_{1.5}O_4$; Mn source

收稿日期:2012-03-22。收修改稿日期:2012-06-13。
国家科技支撑计划(No.2007BAQ01055)、国家自然科学基金(No.50574063)以及四川大学青年基金(No.2011SCU11081)资助项目。
*通讯联系人。E-mail:xiaodong2009@163.com

0 Introduction

Lithium-ion batteries are considered as the most promising energy storage systems owing to their long lifespan and high energy density, with environmentally benign and other advantages[1-3]. With the development of the hybrid electric vehicle and electric vehicles, the high power density is considered to be first and foremost. One approach of increasing the power density of lithium-ion batteries is to enhance its operational voltage by utilizing high-voltage cathodes[4-5]. Because of the highest theoretical discharge capacity with stable cycle ability at this high potential, $LiNi_{0.5}Mn_{1.5}O_4$ (146.7 $mAh \cdot g^{-1}$) material receives the greatest attention for its dominant potential plateau at around 4.7 V[6-7].

The physical and the electrochemical performances of the cathode material are strongly dependent upon the synthesis method. The spinel materials have been synthesized via various methods such as solid-state reaction [8], sol-gel process [9-10], co-precipitation reaction [11] and carbon combustion method[12-13]. Among them, the solid-state reaction is the simplest, but the particle size of the material obtained by this method is non-uniform. For sol-gel method, the final products are very uniform, but the drying time lasts too long and the raw materials cost too much. It is difficult to control the reaction for co-precipitation, and the technology is too complex. Although the carbon combustion process is hard to control, this method allows reactants to mix at atomic or molecular level, and it is the most effective method to prepare the submicron materials, which is adaptable for industrialization. Therefore, carbon combustion process is a promising method to synthesize submicron material efficiently.

In addition, the selection of the reagent is another factor for the performances. Recently, a series of $LiNi_{0.5}Mn_{1.5}O_4$ cathode materials have been prepared via sol-gel method. Their results show that the grain size distribution and electrochemical performances could be significantly influenced by the Li source [14]. Similarly, the selection of starting Mn source is of great importance in the preparation of spinels with better electrochemical behaviors.

In this paper, the spinel cathode material is prepared with sucrose combustion method by using two different Mn sources. The effects of the starting Mn source on physical and electrochemical properties are studied.

1 Experimental

1.1 Preparation of materials

Stoichiometric amounts of $LiNO_3$(99%), $Mn(NO_3)_2$ (50%) or $Mn(CH_3COO)_2 \cdot 4H_2O$(99%), $Ni(NO_3)_2 \cdot 6H_2O$ (98%) were weighed in accordance with $LiNi_{0.5}Mn_{1.5}O_4$, and the mixed solution was prepared by dissolving the above weighed compounds in distilled water. Then, the weighed sucrose as fuel was dissolved in distilled water and slowly added to the mixed solution. Afterwards, the dark green solution was continuously stirred at 30 ℃ water bath for four hours, Yellow brown solution was obtained after two hours by evaporation at 90 ℃, then the surface became foamable and the solution began to expand due to the evolution of gases generated in the thermolysis of the reagents. The foamy solution was heated, and after a few minutes, the solution started to burn up spontaneously without flame, finally, the very light and downy black precursor powders were obtained. The powders were collected and sintered at 900 ℃ for 10 h with the same heating/cooling rate in air to obtain the final products. The prepared materials were denoted as samples A and B for $Mn(NO_3)_2$ and $Mn(CH_3COO)_2 \cdot 4H_2O$ as the Mn source, respectively.

1.2 Physical characterization of materials

The purity and crystalline structure of each sample was analyzed by X-ray diffraction (XRD, DX-1000, Cu $K\alpha$ radiation at scanning angle of 10°~80° and scanning rate of $0.06° \cdot s^{-1}$) (λ=0.154 18 nm) with proportional detector operated at 40 kV and 25 mA. The particle morphology and particle size of the samples were observed by scanning electron microscopy (SEM, SPA400 Seiko Instruments). The particle size distribution was tested by laser particle size distribution tester (JL-6000).

1.3 Electrochemical performance of materials

The cathode was fabricated by positive electrode

composites of 80wt% $LiNi_{0.5}Mn_{1.5}O_4$ (LMNO), 13wt% acetylene black (conducting additive) and 7wt% polyvinylidene fluoride (PVDF, binder) onto an Al foil. After being blended in N-methylpyrrolidinone (NMP), the mixtures were spread uniformly onto a thin Al foil, and its surface must be free from oxide layer before coating with electrode materials, dried in vacuum at 120 ℃ for 15 h and then cut into pieces with diameter of 1.4 cm; thus, the area of the active electrode surface was about 1.54 cm^2. The electrolyte was a 1 mol·L^{-1} solution of $LiPF_6$ in ethylene carbonate (EC) and dimethyl carbonate (DMC) (1:1, by volume), and celgard 2400 as the separator. The coin type cells were assembled in an argon-filled glove box. Galvanostatic charging/discharging tests were operated in the potential range of 3.6~5.2 V and at room temperature (25 ℃) with a battery test system (Neware BTS-610). Cyclic voltammetry (CV) was performed on the positive electrode in the cells described above by a CHI 660C electrochemical work station. CV tests were carried out in voltage range of 3.6 ~5.2 V at a scanning rate of 0.10 mV·s^{-1}. Electrochemical impedance spectrum (EIS) was recorded with a zennium electrochemical workstation in a frequency range of 100 kHz~10 mHz at an open-circuit potential of 2.5 V by applying an AC signal of 5 mV.

2 Results and discussion

2.1 Structure analysis

The X-ray patterns of the samples prepared with different Mn sources are illustrated in Fig.1(a). All the fundamental diffraction peaks from Fig.1(a) could be assigned to a nonstoichiometric cubic spinel structure of $LiNi_{0.5}Mn_{1.5}O_4$(PDF 80-2162) with the space group of *Fd3m*[15], the sharp peaks in the patterns indicate that both samples are well crystallized. When Mn $(CH_3COO)_2 \cdot 4H_2O$ is used as the Mn source for sample B, no impurities phases are detected. However, two peaks at about 37.5° can be observed when $Mn(NO_3)_2$ is used as the Mn source for sample A, being recognized as the impurity phase of NiO (Fig.1(b)), which is consistent with the literature report[16]. This is

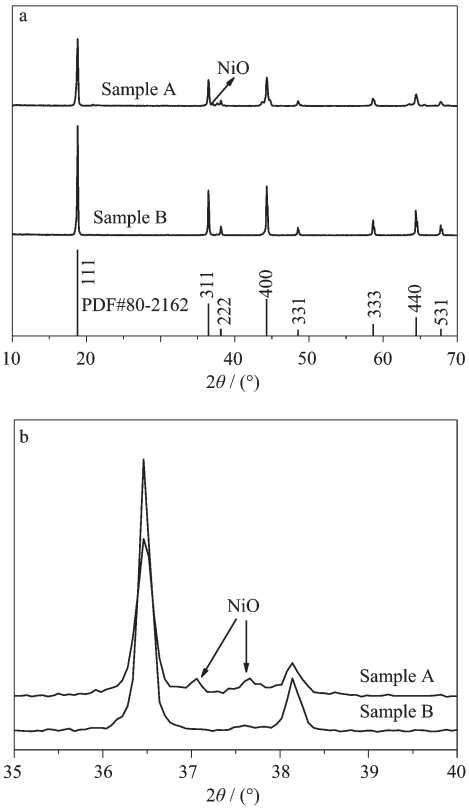

Fig.1 XRD patterns of samples A, B and PDF#80-2162 (a), and patterns for samples A,B in the2θ range of 35°~42°(b).

a common phenomenon resulted from oxygen release when the sintering temperature is above 650 ℃, accompanied with a small amount Mn^{3+} generated for balancing the valence.

The calculated cell lattice parameters of the samples are listed in Table 1. The crystallinity of the two samples synthesized by combustion method are both above 95% (calculated via Jade software), which shows that both samples crystallize well through the above preparation process. Their lattice parameters of a axis are 0.817 11 nm (for sample A) and 0.8170 4 nm (for sample B), greater than the theoretical value 0.817 0 nm. Since the radius of Mn^{3+}(0.065 nm)is larger than that of Mn^{4+}(0.053 nm), as mentioned above, more Mn^{3+} and impurity phase of NiO appear in sample A to balance the valence caused by oxygen loss, so both the lattice parameters (a) and the crystal cell volume of sample A are larger than those of sample B. Therefore, the diffusion pathway of Li ions for sample B is shorter than that of A, which is good for Li ions inserting and

Table 1 Calculated cell parameters of sample A and B

Sample	a / nm	Volume / nm^3	Crystallite size / nm	Crystallinity	$I_{(311)}$ / $I_{(400)}$
Sample A	0.817 11	0.545 56	44.3	95.012%	0.952
Sample B	0.817 04	0.545 41	40.5	98.662%	0.948
PDF 80-2162	0.817 00	0.545 30	/	/	/

extracting. Besides, less Mn^{3+} can reduce the dissolution of manganese, decrease the polarization, and increase the cycle performance. These features can significantly contribute to the electrochemical performances of the materials. The crystallite size both outdistance the lattice parameters (a) testifies that the materials are polycrystalline structures. It has been reported that the intensity ratio of the $I_{(311)}/I_{(400)}$ peaks reflects the structural stability of the $[Mn_2]O_4$ spinel framework[17]. The $I_{(311)}/I_{(400)}$ ratio for samples A and B are higher than 0.9, indicating that these samples show good structural stability.

2.2 Morphological characterization

Fig.2 shows the SEM images of sample A and B. It can be observed that all the samples have sharp edges, with obvious spinels, which suggests that the samples are well crystallized. This is in agreement with the X-ray results. Furthermore, the particles are with narrow particle size distributions and no obvious aggregation. The small particle size of the samples could be explained by the gases generated during the sucrose combustion process and the raw material decomposition, which separate the particles into the spongy and loose morphology of the samples (Fig.2). In addition, the gases spreading out can also help to remove the heat generated by the sources burning, hence, suppressing the agglomeration of the particles. The more gas generated, the smaller particle size can

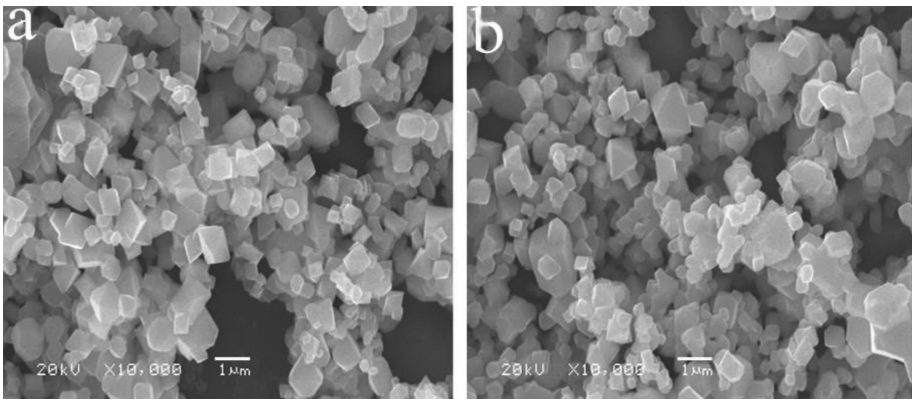

Fig.2 SEM images of samples A and B synthesized by carbon combustion method

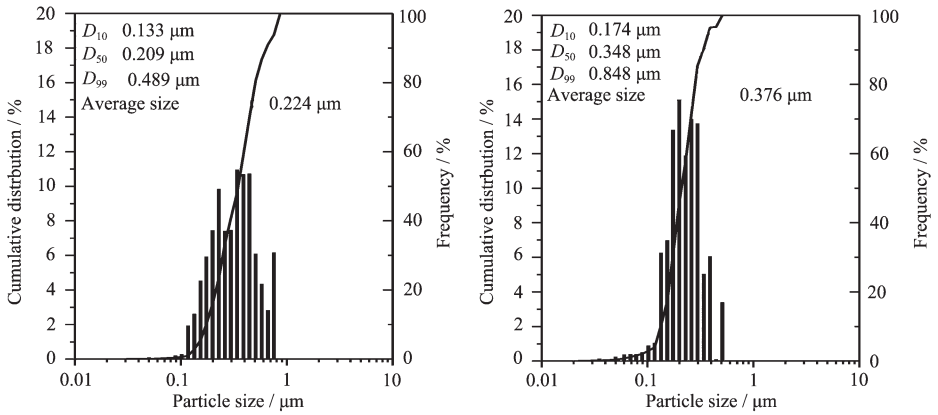

Fig.3 Particle size distribution of sample A and B

be achieved. Fig.3 shows the particle size frequency and cumulative distribution of the samples. The average particle size (D_{50}) of sample A is 0.348 m (Fig.3a), and 0.209 μm (Fig.3b) for sample B. Small particles could supply larger surface area where the electrochemical reaction occurs between the cathode surface and the electrolyte. Moreover, the particle distributions are both narrow, which is in agreement with the SEM images above. This is an important issue for cathode materials because electrode materials with sub-micron particle size can notably improve their electrochemical properties, such as cycle capability and discharge capacity. For the two samples, as there are more gases generated in the combustion process for sample B, it owns smaller particle size and narrower distribution, so, it is expected to exhibit better cycle stability and electrochemical performances.

2.3 Electrochemical test

2.3.1 Cyclic voltammetry analysis

Fig.4(a) shows the cyclic voltammetry (CV) curves of the samples plotted in the potential range from 3.6 V to 5.2 V at a scan rate of 0.1 $mV \cdot s^{-1}$. There are three pairs of redox peaks that can be clearly observed in the CV curves for both samples. They appear at around 4.1 V, 4.7 V and 4.8 V, corresponding to the Mn^{3+}/Mn^{4+}, Ni^{2+}/Ni^{3+} and Ni^{3+}/Ni^{4+}, respectively, which is in good line with the charge-discharge profiles below. Moreover, the redox peak in the potential region from 3.9 V to 4.1 V indicates that the Mn^{3+}ions indeed exist in the cathode material, and the intensity of this peak can reflect the purity to some extent [18]. Since there is more amount of Mn^{3+} resulted from the existence of small amount of NiO for sample A, as a result, the redox peak around 4V is stronger than that of sample B (Fig.4 (b)). Fig.5 shows the cyclic voltammetry (CV) curves of sample B after different cycles. It can be seen that the intensities of the peaks around 4.1 V almost keep the same after different cycles, which are different from the intensities of the peaks around 4.7 V area. It can be observed that the peak intensities at 4.7 V area slowly decrease with cycle number increasing, showing excellent reversibility and no any polazrization when cycling, demonstrating the spinel structure of sample B is very stable with the reversible intercalation/deintercalation of Li^+.

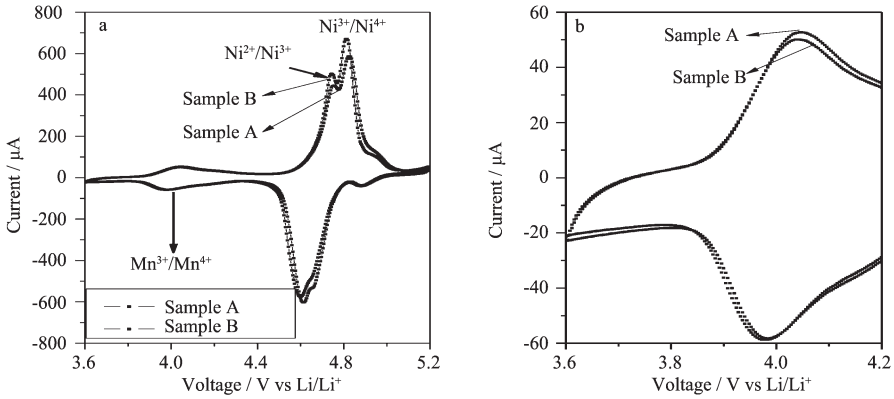

Fig.4　Cyclic voltammetry curves of samples A and B(a), and cyclic voltammetry curves in the voltage range of 3.6~4.2 V for samples A and B(b)

2.3.2 Electrochemical performance

Fig.6 demonstrates the cycle and rate performance of sample A and B at various discharge rates from 1C to 20C (1C=140 mA) between 3.6 and 5.2 V versus Li. It can be clearly seen that the discharge capacities of the two samples are affected by C rates, and their specific capacities are high at low discharge rate and decrease only a little as the rate increases, indicating good rate performances for the spinels. It is obvious that the compound prepared with $Mn(CH_3COO)_2 \cdot 4H_2O$ has better rate performance and higher specific capacity at every discharge rate. On the other hand, both the two samples have excellent cycling stability at each rate, their discharge

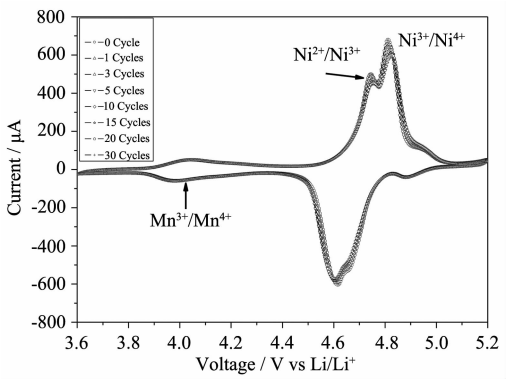

Fig.5 Cyclic voltammetry curves of sample B after different cycles

capacity does not decrease after about twenty cycles at each rate. At 1C, the discharge specific capacities are 141.7 and 144.5 mAh·g^{-1} for sample A and B, respectively, which are very close to the theoretical capacity, as can be seen, the discharge capacities are 132.7 and 136.3 mAh·g^{-1} at 3C, 126.4 and 132 mAh·g^{-1} at 5C, 115.3 and 124.7 mAh·g^{-1} at 10C for samples A and B, respectively. When the current comes to 20C, they are still as high as 84.7 and 96.6 mAh·g^{-1}. Clearly, the capacities of sample B surpass that of sample A at every discharge rate, indicating sample B with $Mn(CH_3COO)_2 \cdot 4H_2O$ exhibits better electrochemical performance. The retentions of both cathodes as a function of discharge rate are calculated based on the capacity of 1C in Table 2. The discharge capacity decays at the beginning low rates for both cathodes are actually slow, and when the current comes to 10C and 20C, the capacity attenuation is accelerated. The capacity retention is 81.4% and 86.3% for 10C, 59.8% and 66.9% for 20C for samples A and B, respectively. Obviously, the electrochemical performance of products can be improved by using manganese acetate as the Mn sources, especially at high discharge rate.

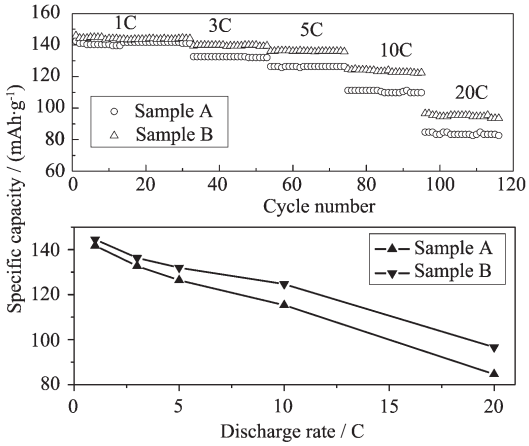

Fig.6 Cycle performances for sample A and B at various discharge rates

Table 2 Calculated capacity retention of sample A and B

Sample	1C	3C	5C	10C	20C
Sample A	100%	93.6%	89.2%	81.4%	59.8%
Sample B	100%	94.3%	91.3%	86.3%	66.9%

The cycling performances of both cathode materials measured at 1C rate at room temperature between 3.6 and 5.2 V versus Li are shown in Fig.7. For both samples A and B, the specific capacities will reach to maximum after about 20 cycles, and remain as 129.1 and 138.1 mAh·g^{-1} for 100 cycles, keeping at 91.1% and 95.6% of the maximum valve, with approximately 0.126 and 0.064 mAh·g^{-1} capacity loss per cycle. It is obvious that the compound prepared with $Mn(CH_3COO)_2 \cdot 4H_2O$ has stable cycling behavior, while the other one presents an obvious capacity decreasing upon cycling. The abrupt capacity decay for sample A can be explained by the impurity phase

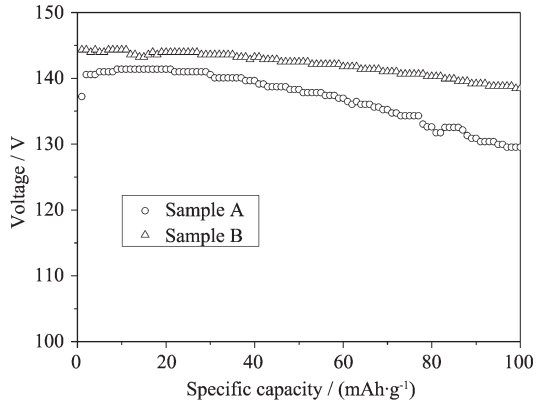

Fig.7 Cycling performance for the samples A and B at 1C

of NiO, larger particle size, wider grain size distribution, and inferior crystallinity. Larger particles could only supply smaller surface area where the electrode reaction occurs between the cathode surface and the electrolyte at the high operating voltage. Combined with the impurity phase of NiO, wide grain size distribution and inferior crystallinity, the spinel material surface is easier to be corroded by HF, which is one of the side products resulted from the electrolyte. This phenomenon can accelerate the solution of transition metal elements and the decomposition of the electrolyte, and finally, the deterioration of cyclability.

Fig.8 shows the charge-discharge curves in a potential range from 3.6 V to 5.2 V of both samples prepared by carbon combustion method. The cell is charged at 1C before discharge test at various rates. It can be seen that the initial charge curves of 1C for both samples exhibit two voltage plateaus. One is apparent at 4.7 V and the other is not obvious at 4.1 V, and the interval between charge and discharge plateau is small, which becomes much bigger as the discharge current increasing. Since the charge plateau keeps almost constant, this phenomenon demonstrates that the discharge plateaus decrease gradually with the C rate increasing, indicating the effect of polarization increases along with the increase of the current.

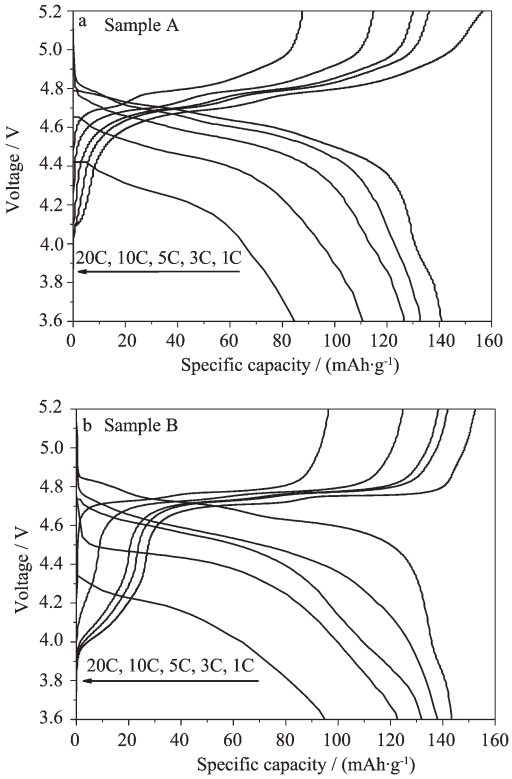

Fig.8 Chargedischarge plateaus for the samples A(a) and B(b) at various discharge rates

2.3.3 Electrochemical impedance spectrum (EIS) analysis

Electrochemical impedance spectrum (EIS) for the discharged cell was measured in the frequency range of 100 kHz~10 mHz. EIS was applied to further analyze the electrochemical performances affected by Mn sources. Before EIS test, the two cells were discharged after 30 cycles at 1C in a voltage range of 3.6~5.2 V. Fig.9 shows that both spectra consist of an intercept at the Z' axis in high frequency, a semicircle in the middle frequency and a straight line in the low frequency region, indicating the resistance of electrolyte and $LiNi_{0.5}Mn_{1.5}O_4$ thin film, the charge-transfer resistance of electrochemical reaction, and the resistance related to the lithium-ion diffusion in the spinels, respectively. An equivalent circuit model of EIS is constructed to analyze the resistance of $LiNi_{0.5}Mn_{1.5}O_4$ electrode(Fig.9b), which can explain the impedance spectra through the ohmic resistance Re,

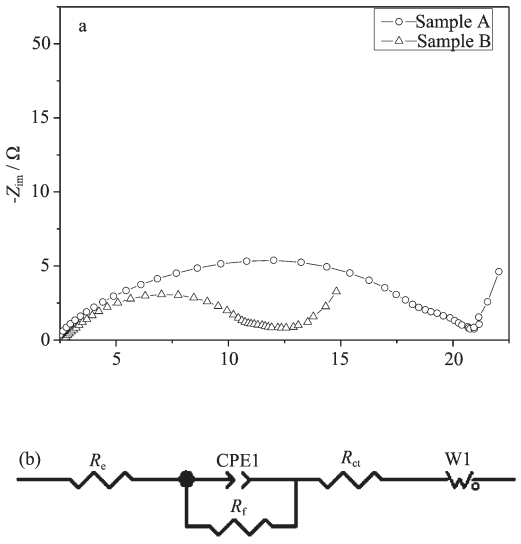

Fig.9 AC impedances for samples A and B (a); Equivalent circuit model for fitting the experimental AC data (b)

Table 3 Numerical values of the elements from equivalent circuit

Sample	R_e / Ω	R_f / Ω	R_{ct} / Ω
A	3.911	18.39	21.56
B	2.722	8.763	11.77

charge-transfer R_f and the diffusion resistance Rct. The parameters of the equivalent circuit by computer simulations are shown in Table 3. As can be seen from the table, the resistance of the electrolyte and sample B thin film is only 2.72 Ω, the charge-transfer resistance of electrochemical reaction is 8.76 Ω, the diffusion resistance is 11.77 Ω. The lower resistance for sample B indicates a lower electrochemical polarization and high electronic transmission rate which is in favor of the transmission of ions and electrolytes, leading to higher electrical conductivity and the optimum electrochemical performance of sample B.

3 Conclusions

In this work, spinel $LiNi_{0.5}Mn_{1.5}O_4$ cathode materials were synthesized with combustion method. The effect of Mn source, on physical and electrochemical properties of $LiNi_{0.5}Mn_{1.5}O_4$ cathode materials is discussed. The results show that the material obtained with manganese acetate has smaller average particle size and narrower particle size distribution, which results in good rate performance and excellent capacity retention. Its discharge capacity is 144.5 $mAh \cdot g^{-1}$, capacity retention is 95.6% after 100 cycles in the cut-off voltage of 3.6~5.2 V, and high discharge capacities of 136.3, 132, 124.7 and 96.6 $mAh \cdot g^{-1}$ are obtained at the rate of 3, 5, 10 and 20C, respectively. The results indicate that manganese acetate is an excellent Mn source for the preparation of spinel $LiNi_{0.5}Mn_{1.5}O_4$ cathode materials with combustion method.

Acknowledgements: This work was funded by the National Scientific and Technical Backup Plan of China (No. 2007BAQ01055) and Youth Foundation of Sichuan University (No.2011SCU11081). We would like also to thank the Analysis and Test Center, Polymer Engineering National Key Laboratory of Sichuan University for their support in characterization and measurement.

References:

[1] Guo X D, Zhong B H, Liu H, et al. *J. Electrochem. Soc*., **2009**,**156**:A787-A790

[2] TANG Yan(唐艳), ZHONG Ben-He(钟本和), GUO Xiao-Dong(郭孝东), et al. *Acta Phys.-Chim. Sin.*(*Wuli Huaxue Xuebao*), **2011**,**27**(4):869-874

[3] Wolfgang M, Jean-Francios C, Dietrich G, et al. *Electrochimica Acta*, **2010**,**55**:4964-4969

[4] Liu G Q, Wen L, Liu Y M. *J. Solid State Electrochem.*, **2010**,**14**:2191-2202

[5] Chi L H, Dinh N N, Brutti S, et al. *Electrochimica Acta.*, **2010**,**55**:5110-5116

[6] Yi T F, Zhu Y R, Zhu R S. *Solid State Ionics*., **2008**,**179**: 2132-2136

[7] Mohamed A, Jose M A, Rosa M, et al. *J. Power Sources*, **2008**,**185**:501-511

[8] CHEN Zhao-Yong(陈召勇), XIAO Jing(肖劲), ZHU Hua-Li(朱华丽), et al. *Chinese J. Inorg. Chem.*(*Wuji Huaxue Xuebao*), **2005**,**21**(9):1417-1421

[9] Yang T Y, Sun K, Lei Z Y, et al. *J. Alloys Compd.*, **2010**, **502**:215-219

[10]Liu H Y, Wu Y P, Rahm E, et al. *J. Solid State Electrochem*., **2004**,**8**:450-466

[11]Chang Z R, Dai D M, Tang H W, et al. *Electrochimica Acta*, **2010**,**55**:5506-5510

[12]DAI Ke-Hua(代克化), MAO Jing(毛景), ZHAI Yu-Chun(翟玉春). *Acta Phys.-Chim. Sin.*(*Wuli Huaxue Xuebao*), **2010**,**26**(8):2130-2134

[13]HE Ze-Qiang(何则强), XIONG Li-Zhi(熊利芝), WU Xian-Ming(吴显明), et al. *Chinese J. Inorg. Chem.*(*Wuji Huaxue Xuebao*), **2007**,**23**(5): 875-878

[14]Yang T Y, Sun K N, Lei Z Y, et al. *J. Solid State Electrochem.*, **2011**,**15**:391-397

[15]Feng X Y, Shen C, Fang X, et al. *J. Alloys Compd.*,**2011**, **509**:3623-3626

[16]PANG Pei-Pei(庞佩佩), TANG Zhi-Yuan(唐致远), YUAN Xiu-Lan(袁秀兰). *J. Chinese Battery Industry.*(*Dianchi Gongye*),**2010**,**15**(3):160-164

[17]Fang X, Ding N, Feng X Y, et al. *Electrocheimica Acta*, **2009**,**54**:7471-7475

[18]Yi T F, Shu J, Zhu Y R, et al. *J. Phys. Chem. Solids*, **2009**,**70**:153-158